

$K^+\Lambda$ electroproduction above the resonance region

Tom Vrancx,^{*} Jan Ryckebusch,[†] and Jannes Nys[‡]

Department of Physics and Astronomy,
Ghent University, Proeftuinstraat 86, B-9000 Gent, Belgium

(Dated: May 27, 2014)

Background: In π^+n and π^-p electroproduction, conventional models cannot satisfactorily explain the data above the resonance region, in particular the transverse cross section. Although no high-energy $L-T$ -separated cross-section data is available to date, a similar scenario can be inferred for $K^+\Lambda$ electroproduction.

Purpose: Develop a phenomenological model for the $p(\gamma^*, K^+)\Lambda$ reaction at forward angles and high-energies. Propose a universal framework for interpreting charged-kaon and charged-pion electroproduction above the resonance region.

Method: Guided by the recent model for charged-pion electroproduction, developed by the authors, a framework for $K^+\Lambda$ electroproduction at high energies and forward angles is constructed. To this end, a Reggeized background model for $K^+\Lambda$ photoproduction is first developed. This model is used as a starting base to set up an electroproduction framework.

Results: The few available data of the unseparated $p(\gamma^*, K^+)\Lambda$ cross section are well explained by the model. Predictions for the $L-T$ -separation experiment planned with the 12 GeV upgrade at Jefferson Lab are given. The newly-proposed framework predicts an increased magnitude for the transverse structure function, similar to the situation in charged-pion electroproduction.

Conclusions: Within a hadronic framework featuring Reggeized background amplitudes, s -channel resonance-parton effects can explain the observed magnitude of the unseparated $p(\gamma^*, K^+)\Lambda$ cross section at high energies and forward angles. Thereby, no hardening of the kaon electromagnetic form factor is required.

PACS numbers: 13.40.Gp, 13.60.Le, 24.10.-i, 25.30.Rw

I. INTRODUCTION

Above the resonance region, the transverse cross section σ_T measured in charged-pion electroproduction is significantly larger than predicted by regular hadronic models [1]. In Ref. [2], Kaskulov and Mosel proposed a framework explaining this observation. In the Kaskulov-Mosel formalism, the missing transverse strength is provided by the residual effects of nucleon resonances in the gauge-fixing s (or u) channel.

It is argued that such contributions become more important for increasing intermediate-proton and photon virtualities. Indeed, above the resonance region the proton is highly off-shell and the contributions from more massive intermediate states increase in importance. With growing intermediate-proton virtuality, also the hardening of the resonance electromagnetic transition can be anticipated to play an increasingly important role. This results in a dual viewpoint in which the residual effects can be interpreted as originating from the partonic picture of hadrons.

The resonance-parton (R-P) contributions are effectively implemented by means of an electromagnetic (EM) transition form factor for the proton in the s channel. In Ref. [3], a new version of this form factor was proposed which has a simple physical interpretation and respects the correct on-shell limit. The resulting model was dubbed the “Vrancx-Ryckebusch” (VR) model and offers an explanation for the high-energy, forward-angle π^+n and π^-p electroproduction data, thereby covering a wide range of invariant masses ($2 \text{ GeV} \lesssim W \lesssim 4 \text{ GeV}$) and photon virtualities ($0.2 \text{ GeV}^2 \lesssim Q^2 \lesssim 5 \text{ GeV}^2$).

From the observations in the pion case, along with SU(3) symmetry considerations, one may infer that an increased transverse response might also occur in charged-kaon electroproduction. Within the VR framework, this can be anticipated from the employed strategy of introducing an effective EM transition form factor for the proton in the s channel, accounting for the R-P contributions.

To this day, no σ_T data is available for high-energy $K^+\Lambda$ electroproduction and it is to be awaited if its magnitude is larger than expected. In this regard it is worth noting that the measured $p(\gamma^*, K^+)\Lambda$ unseparated cross section σ_u at high energies can be reproduced by the Vanderhaeghen-Guidal-Laget (VGL) model [4–7] after introducing an effective kaon EM form factor. The kaon EM cutoff energy employed in the VGL model is significantly increased compared to the value extracted from elastic eK scattering. This may hint at an anomalously large transverse contribution to the unseparated cross section. After completing the 12 GeV upgrade at Jefferson Lab (JLab), one plans to measure the first $p(\gamma^*, K^+)\Lambda$ separated structure functions σ_L and σ_T at high energies [8].

Following the strategy employed in charged-pion electroproduction [3], the VR model for high-energy forward-angle $K^+\Lambda$ electroproduction will be developed. In Sec. II, the transition currents are discussed. These will be used in Sec. III to construct an improved model for high-energy, forward-angle $K^+\Lambda$ photoproduction. Starting from this photoproduction model, the VR model will be derived in Sec. IV. There, predictions will be presented for the above-mentioned experiment planned at JLab [8]. In Sec. V, the conclusions of this work will be given.

^{*} Tom.Vrancx@UGent.be

[†] Jan.Ryckebusch@UGent.be

[‡] Jannes.Nys@UGent.be

II. TRANSITION CURRENTS

In complete analogy to the pion case [3], the adopted current for the gauged pseudoscalar-kaon exchange in $p(\gamma^*, K^+)\Lambda$ is given by

$$(J_K)_{\lambda_p, \lambda_\Lambda}^\mu(s, t, Q^2) = ig_{K\Lambda p} \bar{u}_{\lambda_\Lambda}(p') \gamma_5 \left(F_{\gamma KK}(Q^2) \mathcal{P}_K(t, s) (2k' - q)^\mu + F_p(Q^2, s) \mathcal{P}'_K(t, s, Q^2) \frac{t - m_K^2}{s - m_p^2} (\not{p} + \not{q} + m_p) \gamma^\mu \right) u_{\lambda_p}(p). \quad (1)$$

Here, p , q , k' , and p' are the four-momenta of the nucleon, of the virtual photon, of the kaon, and of the hyperon in the center-of-mass frame.¹ The Mandelstam variables (s, t, u) are defined in the standard way. The proton and Λ polarizations are denoted by λ_p and λ_Λ , and the strong $K\Lambda p$ coupling constant by $g_{K\Lambda p}$. Note the absence of the $\text{SU}(2)$ $\sqrt{2}$ factor in J_K , compared to the pion-exchange current of Ref. [3]. The employed expression for the kaon-Regge propagator $\mathcal{P}_K(t, s)$ reads

$$\mathcal{P}_K(t, s) = -\alpha'_K \varphi(\alpha_K(t)) \Gamma(-\alpha_K(t)) \left(\frac{s}{s_0} \right)^{\alpha_K(t)}. \quad (2)$$

Following the convention of the VGL [4–7] and the Regge-plus-Resonance (RPR) [9–12] models, the “mass scale” s_0 is fixed to $s_0 = 1 \text{ GeV}^2$. In Ref. [3], the convention $s_0 = 1/\alpha'$ is adopted. The model assumptions with regard to the Regge trajectories $\alpha(t)$ and Regge phases $\varphi(\alpha(t))$, will be discussed in Sec. III A. The EM form factors $F_{\gamma KK}(Q^2)$ and $F_p(Q^2, s)$, and the modified kaon-Regge propagator $\mathcal{P}'_K(t, s, Q^2)$ will be discussed in Sec. IV A. At this point, it suffices to note that at vanishing photon virtuality ($Q^2 = 0$) it holds that $F_{\gamma KK}(Q^2 = 0) = F_p(Q^2 = 0, s) = 1$ and $\mathcal{P}'_K(t, s, Q^2 = 0) \equiv \mathcal{P}_K(t, s)$.

The expressions for the vector (V , $J^P = 1^-$) and axial-vector (A , $J^P = 1^+$) transition currents J_{K_V} and J_{K_A} are adopted from Ref. [2] and read

$$(J_{K_V})_{\lambda_p, \lambda_\Lambda}^\mu(s, t, Q^2) = G_{\gamma K_V K} G_{K_V \Lambda p} F_{\gamma K_V K}(Q^2) \mathcal{P}_{K_V}(t, s) \varepsilon^{\mu\nu\sigma\tau} q_\nu k_\sigma \times \bar{u}_{\lambda_\Lambda}(p') \left((1 + \kappa_{K_V \Lambda p}) \gamma_\tau - \frac{\kappa_{K_V \Lambda p}}{2m_p} (p + p')_\tau \right) u_{\lambda_p}(p), \quad (3)$$

and

$$(J_{K_A})_{\lambda_p, \lambda_\Lambda}^\mu(s, t, Q^2) = -i G_{\gamma K_A K} G_{K_A \Lambda p} F_{\gamma K_A K}(Q^2) \mathcal{P}_{K_A}(t, s) (k^\mu q^\nu - q^\sigma k_\sigma g^{\mu\nu}) \times \bar{u}_{\lambda_\Lambda}(p') \left((1 + \kappa_{K_A \Lambda p}) \gamma_\nu - \frac{\kappa_{K_A \Lambda p}}{2m_p} (p + p')_\nu \right) \gamma_5 u_{\lambda_p}(p). \quad (4)$$

Note that the $\sqrt{2}$ factor was dropped again, and that a minus sign missing in Ref. [2], was added to the right-hand side of Eq. (4). The EM coupling constant is represented by $G_{\gamma K_V A K}$, and the standard vector and anomalous tensor coupling constants by $G_{K_V A \Lambda p}$ and $\kappa_{K_V A \Lambda p}$. The vector and axial-vector Regge propagators have the same functional dependence and are given by

$$\mathcal{P}_{K_V A}(t, s) = -\alpha'_{K_V A} \varphi(\alpha_{K_V A}(t) - 1) \Gamma(1 - \alpha_{K_V A}(t)) \left(\frac{s}{s_0} \right)^{\alpha_{K_V A}(t) - 1}. \quad (5)$$

The EM transition form factors $F_{\gamma K_V A K}(Q^2)$ will be discussed in Sec. IV A. As for the form factors $F_{\gamma KK}(Q^2)$ and $F_p(Q^2, s)$ in Eq. (1), it holds that $F_{\gamma K_V A K}(0) = 1$.

III. HIGH-ENERGY $K^+ \Lambda$ PHOTOPRODUCTION

A. A third Regge trajectory

In the kaon sector, the two most important Regge trajectories are the $K(494)$ (pseudoscalar) and $K^*(892)$ (vector) trajectories [13]. These can be parametrized as [9]

$$\alpha_K(t) = \alpha'_K(t - m_K^2), \quad (6)$$

$$\alpha_{K^*}(t) = 1 + \alpha'_{K^*}(t - m_{K^*}^2), \quad (7)$$

with $\alpha'_K = 0.70 \text{ GeV}^{-2}$ and $\alpha'_{K^*} = 0.85 \text{ GeV}^{-2}$. Both the VGL and the RPR model feature these two trajectories and have established that they are essential for the description of $K^+ \Lambda$ photo- and electroproduction.

In Refs. [11, 12], the Regge background for the $p(\gamma, K^+) \Lambda$ reaction was determined from the recent differential cross section and recoil polarization data by the CEBAF Large Acceptance Spectrometer (CLAS) Collaboration [16].² More specifically, a Bayesian analysis was performed for the high-energy ($W > 2.6 \text{ GeV}$) and forward-angle ($\cos \theta_K^* > 0.35$) part of these CLAS data (262 data points) to determine the Regge model variant with the highest evidence. Here, $W = \sqrt{s}$ is the invariant mass and θ_K^* the kaon scattering angle in the center-of-mass frame. It was found that the best model, dubbed “Regge-2011”, features rotating phases for both the K and K^* trajectories. For this model, a $\chi^2_{\text{NDF}} = 3.15$ is obtained for the description of the high-energy and forward-angle $p(\gamma, K^+) \Lambda$ CLAS data [11, 12]. As there is definitely room for improvement, the possibility is exploited of introducing a third Regge trajectory contributing to the $p(\gamma^{(*)}, K^+) \Lambda$ reaction. In this regard, two candidates are considered: the $K_1(1400)$ (axial-vector) and the $K^*(1410)$ (vector) trajectory [13]. These are parametrized as [14, 15]

$$\alpha_{K_1(1400)}(t) = 1 + \alpha'_{K_1(1400)}(t - m_{K_1(1400)}^2), \quad (8)$$

¹ In Ref. [3], these four-momenta are also defined in the center-of-mass frame and not in the laboratory frame, as mentioned.

² In Table IV of Ref. [12], an overview is given of the available $p(\gamma, K^+) \Lambda$ data.

TABLE I. Coupling constants and corresponding χ^2_{NDF} values of the three-trajectory Regge model variants featuring a K , a K^* and a $K_1(1400)$ trajectory. Results are listed for a rotating K trajectory and all phase combinations for the K^* and K_1 . For the sake of reference also the results of the two-trajectory Regge-2011 model are shown. The models were optimized against the high energy ($W > 2.6$ GeV) and forward-angle ($\cos \theta_K^* > 0.35$) CLAS data for the $p(\gamma, K^*)\Lambda$ differential cross section and recoil polarization (262 data points) [16].

Model	$\{\varphi_K, \varphi_{K^*}, \varphi_{K_1(1400)}\}$	$g_{K\Lambda p}$	$G_{\gamma K^* K} G_{K^* \Lambda p}$ (GeV $^{-1}$)	$\kappa_{K^* \Lambda p}$	$G_{\gamma K_1(1400) K} G_{K_1(1400) \Lambda p}$ (GeV $^{-1}$)	$\kappa_{K_1(1400) \Lambda p}$	χ^2_{NDF}
Ia	$\{R, C, C\}$	-12.2	-0.29	50	32.3	-1.35	17.1
IIa	$\{R, R, C\}$	-13.2	-9.84	1.51	16.5	-0.86	2.58
IIIa	$\{R, C, R\}$	-10.8	-0.44	50	28.0	-1.74	13.6
IVa	$\{R, R, R\}$	-12.6	-10.5	1.38	7.48	-0.19	2.99
Regge-2011	$\{R, R, -\}$	-12.9	-10.8	1.77	—	—	3.15

TABLE II. As in Table I, but for the model based on a third $K^*(1410)$ trajectory instead of a $K_1(1400)$ trajectory.

Model	$\{\varphi_K, \varphi_{K^*}, \varphi_{K^*(1410)}\}$	$g_{K\Lambda p}$	$G_{\gamma K^* K} G_{K^* \Lambda p}$ (GeV $^{-1}$)	$\kappa_{K^* \Lambda p}$	$G_{\gamma K^*(1410) K} G_{K^*(1410) \Lambda p}$ (GeV $^{-1}$)	$\kappa_{K^*(1410) \Lambda p}$	χ^2_{NDF}
Ib	$\{R, C, C\}$	-13.2	-0.01	0.03	41.6	-0.53	6.33
IIb	$\{R, R, C\}$	-13.2	-6.79	1.04	32.7	0.70	1.06
IIIb	$\{R, C, R\}$	-12.4	-0.23	50	49.3	-0.46	4.91
IVb	$\{R, R, R\}$	-14.2	-19.4	0.68	-54.4	-0.55	2.04
Regge-2011	$\{R, R, -\}$	-12.9	-10.8	1.77	—	—	3.15

$$\alpha_{K^*(1410)}(t) = 1 + \alpha'_{K^*(1410)}(t - m_{K^*(1410)}^2), \quad (9)$$

with $\alpha'_{K_1(1400)} = 0.75$ GeV $^{-2}$ and $\alpha'_{K^*(1410)} = 0.83$ GeV $^{-2}$. All the trajectories considered here are degenerate. This means that the corresponding Regge phases can either be constant (C) or be rotating (R):

$$\varphi(\alpha(t)) = \begin{cases} 1 & C, \\ e^{-i\pi\alpha(t)} & R. \end{cases} \quad (10)$$

B. Parameter constraints

Since the phases of the Regge trajectories considered here can be either constant or rotating, there are 8 possible variants for each three-trajectory model. These models, however, are all restricted to some extent as the K and K^* coupling constants must meet certain constraints, based on symmetry arguments. The strong coupling $g_{K\Lambda p}$ can be inferred from the strong pion-nucleon coupling $g_{\pi NN}$ by means of SU(3) symmetry:

$$g_{K\Lambda p} = -\frac{1}{\sqrt{3}}(3 - 2\alpha_D)g_{\pi NN}, \quad (11)$$

with $\alpha_D = 0.644$ the experimentally determined SU(3) symmetric coupling fraction. By allowing a 20% breaking of SU(3) symmetry and taking into account the uncertainty on the pion-nucleon coupling, i.e. $g_{\pi NN} \approx 13.0$ – 13.5 [3], the following limits on $g_{K\Lambda p}$ emerge:

$$-16.0 \leq g_{K\Lambda p} \leq -10.3. \quad (12)$$

The EM coupling constant $G_{\gamma K^* K}$ can be estimated from the decay width of $K^* \rightarrow K\gamma$ [4]:

$$\Gamma_{K^* \rightarrow K\gamma} = \frac{\alpha_e}{24} \frac{G_{\gamma K^* K}^2}{m_{K^*}^3} (m_{K^*}^2 - m_K^2)^3, \quad (13)$$

with α_e the fine-structure constant. From the experimentally determined value $\Gamma_{K^* \rightarrow K\gamma} = 50 \pm 5$ keV [13] one obtains

$$G_{\gamma K^* K} = 0.834 \pm 0.042 \text{ GeV}^{-1}. \quad (14)$$

Also the strong vector and tensor couplings $G_{K^* \Lambda p}$ and $\kappa_{K^* \Lambda p}$ can be related to $G_{\rho NN}$ and $\kappa_{\rho NN}$ through SU(3) symmetry. However, following the arguments given in Ref. [4], only the

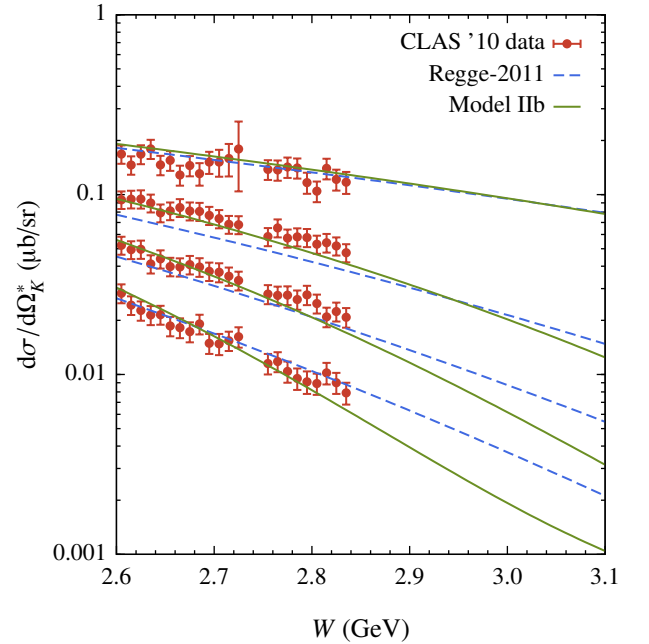


FIG. 1. (Color online) The W dependence of the $p(\gamma, K^*)\Lambda$ unpolarized differential cross section for (from bottom to top) $\cos \theta_K^* = 0.50, 0.60, 0.70, 0.86$ – 0.87 . Predictions from the Regge-2011 model and model IIb are shown. The data are from Ref. [16].

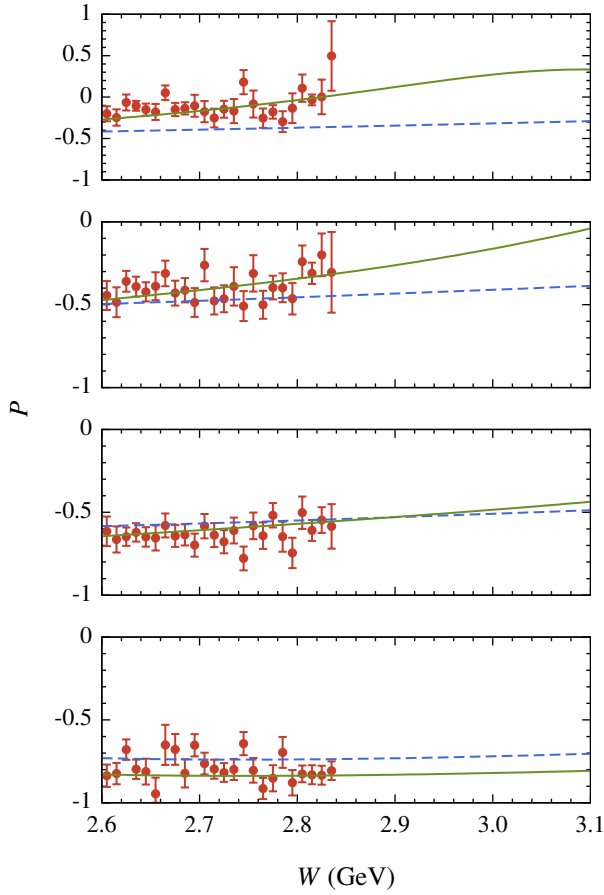


FIG. 2. (Color online) The W dependence of the $p(\gamma, K^+)\Lambda$ recoil polarization P for (from bottom to top) $\cos \theta_K^* = 0.50, 0.60, 0.70, 0.86\text{--}0.87$. Predictions from the Regge-2011 model and model IIb are shown. Curve notations of Fig. 1 are used. The data are from Ref. [16].

predicted signs for the vector and tensor couplings will be respected:

$$G_{K^*\Lambda p} < 0, \quad \kappa_{K^*\Lambda p} > 0. \quad (15)$$

Due to the lack of relevant experimental information, no constraints are imposed on the $K_1(1400)$ and $K^*(1410)$ coupling constants.

C. Results

Tables I and II list the best-fit parameters of the three-trajectory model variants. The coupling constants are optimized against the high-energy and forward-angle CLAS data and respect the constraints of Eqs. (12) and (15). Only the models featuring a rotating K trajectory are listed, as those with a constant K trajectory are not compatible with the data. Indeed, a constant phase for the K trajectory leads to $\chi_{\text{NDF}}^2 = 32.5\text{--}35.2$ for the $K_1(1400)$ model variants, and to $\chi_{\text{NDF}}^2 = 17.2\text{--}34.1$ for the $K^*(1410)$ model variants.

The models with a rotating K and constant K^* phase are systematically in poorest agreement with the data. In fact, these models yield coupling constants approaching the maximum values allowed during the optimization process: models Ia, IIIa, and IIIb yield $\kappa_{K^*\Lambda p} = 50$, and model Ib yields $G_{\gamma K^* K} G_{K^*\Lambda p} = -0.01 \text{ GeV}^{-1}$. This implies that the analyzed CLAS data exclude a constant K^* phase given the constraints of Eq. (15).

Amongst the models with a rotating K^* phase, those with a $K^*(1410)$ (vector) trajectory perform better than those with an $K_1(1400)$ (axial-vector) trajectory. Model IIb clearly stands out from the rest and is in excellent agreement with the data ($\chi_{\text{NDF}}^2 = 1.06$). This model features a constant $K^*(1410)$ and rotating K and K^* trajectories. Note that the value $g_{K\Lambda p} = -13.2$ for this model coincides with the predicted SU(3) value, given the uncertainty on $g_{\pi NN}$. This is also the case for the Regge-2011 model. The employed CLAS data, along with the corresponding predictions of the Regge-2011 model and model IIb, are shown in Figs. 1 and 2 for four $\cos \theta_K^*$ bins. Model IIb constitutes the basis for the VR model, which will be discussed in the forthcoming section.

IV. HIGH-ENERGY $K^+\Lambda$ ELECTROPRODUCTION

A. Form factors

As the $Q^2 = 0$ limit of the proposed $p(\gamma^*, K^+)\Lambda$ model has been established, the Q^2 -dependent quantities in the transition

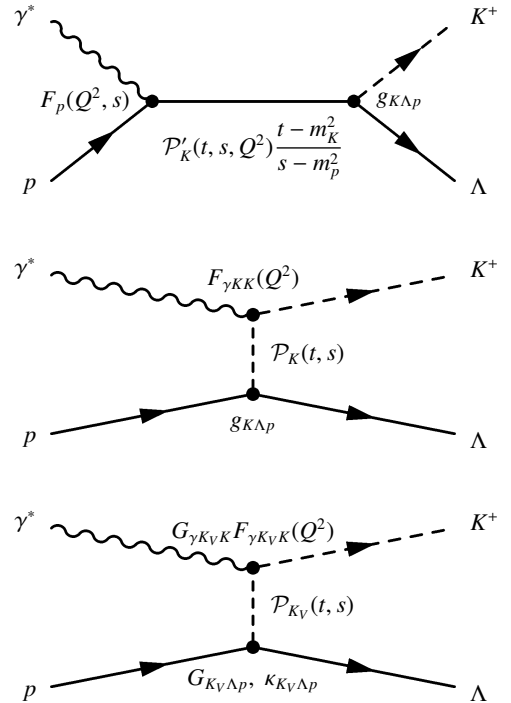


FIG. 3. The gauge-fixing s -channel diagram and the Reggeized pseudoscalar and vector t -channel diagrams that constitute the VR model for $K^+\Lambda$ electroproduction above the resonance region.

current operators of Eqs. (1) and (3) can now be examined. Pursuing the analogy to the VR model for pion electroproduction, an antishrinkage effect is introduced in the s -channel gauge-fixing term of the kaon transition current (1). To this end, the Regge propagator $\mathcal{P}'_K(t, s, Q^2)$ in Eq. (1) is defined as in Eq. (2), but with an altered Regge slope:

$$\alpha'_K \rightarrow \alpha'_K(Q^2, s) = \frac{\alpha'_K}{1 + a \frac{Q^2}{s}}. \quad (16)$$

Here, a is the corresponding dimensionless slope parameter, which has yet to be determined. Figure 3 depicts the s - and t -channel diagrams which constitute the VR model for $p(\gamma^*, K^+)\Lambda$.

A monopole form is adopted for the elastic kaon EM form factor $F_{\gamma KK}(Q^2)$ in of Eq. (1) with a kaon cutoff energy $\Lambda_{\gamma KK}$:

$$F_{\gamma KK}(Q^2) = \left(1 + \frac{Q^2}{\Lambda_{\gamma KK}^2}\right)^{-1}. \quad (17)$$

As the root-mean-square charge radius of the K is experimentally determined as [13]

$$\sqrt{\langle r_K^2 \rangle} = 0.560 \pm 0.031 \text{ fm}, \quad (18)$$

the corresponding monopole cutoff energy is

$$\Lambda_{\gamma KK} = \sqrt{\frac{6}{\langle r_K^2 \rangle}} = 863 \pm 48 \text{ MeV}. \quad (19)$$

In the vector-meson dominance (VMD) model, the kaon EM form factor receives contributions from primarily the ρ , ω , and ϕ mesons [17]:

$$F_{\gamma KK}^{\text{VMD}}(Q^2) = \frac{1}{N} \sum_{v=\rho, \omega, \phi} \frac{g_{vKK}}{f_v} \frac{1}{1 + Q^2/m_v^2}, \quad (20)$$

with $N = \sum_{v=\rho, \omega, \phi} \frac{g_{vKK}}{f_v}$ a normalization constant. Assuming an exact SU(3) flavor symmetry, the EM and strong ω and ϕ coupling constants can be related to those of the ρ :

$$\begin{aligned} f_\omega &= 3f_\rho, & g_{\omega KK} &= g_{\rho KK}, \\ f_\phi &= -\frac{3}{\sqrt{2}}f_\rho, & g_{\phi KK} &= -\sqrt{2}g_{\rho KK}. \end{aligned} \quad (21)$$

From these SU(3) coefficients and the masses of the ρ , ω , and ϕ mesons [13], the VMD monopole cutoff energy for the K is calculated as

$$\Lambda_{\gamma KK}^{\text{VMD}} = \left(-\frac{dF_{\gamma KK}^{\text{VMD}}(Q^2)}{dQ^2} \Big|_{Q^2=0} \right)^{-1/2} \approx 838 \text{ MeV}, \quad (22)$$

which is consistent with the experimental value of Eq. (19).

The form factors $F_{\gamma K_V K}(Q^2)$ in Eq. (3) describe the EM transitions of the vector-kaon trajectories to the outgoing pseudoscalar kaon. For these form factors a monopole form (17) is also adopted. No data is available for the cutoff energies $\Lambda_{\gamma K^* K}$ and $\Lambda_{\gamma K^{*(1410)} K}$, however, so one has to rely on

the corresponding VMD predictions. The VMD description requires the following replacement in expression (20):

$$g_{vKK} \rightarrow G_{vK_V K}. \quad (23)$$

As the K_V are nothing but orbitally excited states of the K , the same SU(3) constraints (21) apply to the strong coupling constants $G_{vK_V K}$:

$$\begin{aligned} G_{\omega K_V K} &= G_{\rho K_V K}, \\ G_{\phi K_V K} &= -\sqrt{2}G_{\rho K_V K}. \end{aligned} \quad (24)$$

Therefore, the K^* and $K^{*(1410)}$ EM transition form factors in the VMD model are identical and equal to $F_{\gamma KK}^{\text{VMD}}(Q^2)$. Consequently, the value of Eq. (22) will be used for the corresponding cutoff energies:

$$\Lambda_{\gamma K_V K} = 838 \text{ MeV}. \quad (25)$$

Note that the above reasoning also applies to axial-vector kaons.

The form factor $F_p(Q^2, s)$ in Eq. (1) describes the EM transition of an on-shell to an off-shell proton with squared four-momentum s , induced by a virtual photon. In the VR model for pion electroproduction, $F_p(Q^2, s)$ is a dipole [3]:

$$F_p(Q^2, s) = \left(1 + \frac{Q^2}{\Lambda_{\gamma pp^*}^2(s)}\right)^{-2}, \quad (26)$$

with an s -dependent cutoff energy ($s \geq m_p^2$)

$$\Lambda_{\gamma pp^*}(s) = \Lambda_{\gamma pp} + (\Lambda_\infty - \Lambda_{\gamma pp}) \left(1 - \frac{m_p^2}{s}\right). \quad (27)$$

Here, $\Lambda_{\gamma pp} = 840 \text{ MeV}$ is the on-shell proton EM cutoff energy. The asymptotic, off-shell proton cutoff energy was determined as $\Lambda_\infty = 2194 \text{ MeV}$ [3].

B. Results

The value of a in Eq. (16) is the only parameter left in the VR model and is fitted to the scarce high-energy, forward-angle $p(\gamma^*, K^+)\Lambda$ data. In order to tune the VR model for pion electroproduction, data with $-t \lesssim 0.5 \text{ GeV}^2$ was used [3]. As few $p(\gamma^*, K^+)\Lambda$ data are available that cover the high-energy region, this range will be extended to $-t < 1 \text{ GeV}^2$. For the same reason the minimum W value will be decreased from 2.6 GeV (Sec. III) to 2.5 GeV. There are 25 published data points that meet these kinematic restrictions: 9 data points measured at Cornell in the seventies [18–20] and 16 recent data points from CLAS [21]. Most of the $p(\gamma^*, K^+)\Lambda$ data are available at $W < 2.5 \text{ GeV}$, recent examples of which can be found in Refs. [22–26]. For the 25 high-energy and forward-angle data points, the optimum value for the slope parameter is found to be

$$a = 2.43. \quad (28)$$

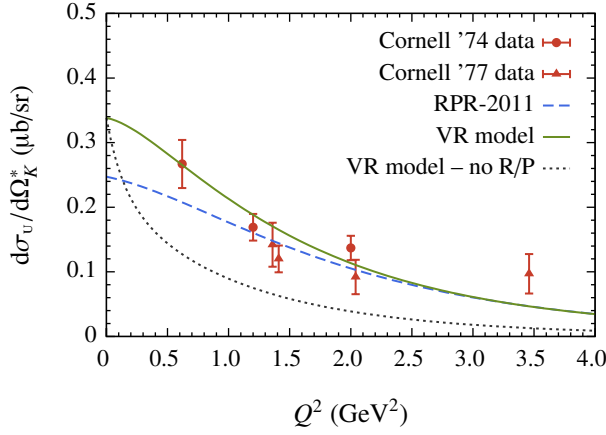


FIG. 4. (Color online) The Q^2 dependence of the $p(\gamma^*, K^+)\Lambda$ unseparated cross section $d\sigma_u/d\Omega_K^*$. Predictions from the RPR model, the VR model, and the VR model without R-P contributions ($\Lambda_\infty = \Lambda_{\gamma pp}$ and $a = 0$) are shown for $W = 2.70$ GeV, $\cos\theta_K^* = 0.98$, and $\varepsilon = 0.86$, which are the averaged kinematics for the different datasets [18, 19].

Remarkably, this value coincides with the one obtained in the pion case [3]. With $\chi^2_{\text{NDF}} = 2.93$, the resulting VR model provides a fair description of the considered $p(\gamma^*, K^+)\Lambda$ data. A word of caution is in order, given the scarcity of the data and the fact that they cover a rather limited W range.

Figures 4 and 5 show 23 of the 25 employed data points, along with the corresponding predictions of the VR and RPR-2011 models. The RPR-2011 model is a prototypical example of a single-channel model, designed to describe the $p(\gamma^*, K^+)\Lambda$ reaction both in and beyond the resonance region [11, 12]. It yields $\chi^2_{\text{NDF}} = 3.58$ for the high-energy $p(\gamma^*, K^+)\Lambda$ data considered. In addition to the t -channel Regge-2011 background discussed in Sec. III A, RPR-2011 features the exchange of the nucleon resonances $S_{11}(1535)$, $S_{11}(1650)$, $F_{15}(1680)$, $P_{13}(1720)$, $D_{13}(1900)$, $P_{13}(1900)$, $P_{11}(1900)$, and $F_{15}(2000)$, in the s channel. For $W \gtrsim 2$ GeV, the effects of these resonances is rather modest.

The VR model is in good agreement with the 19 σ_u data points. For $Q^2 \lesssim 2$ GeV², the VR model predicts larger σ_u cross sections than Regge-2011. Both models predict a similar σ_u for $3 \lesssim Q^2 \lesssim 4$ GeV², but have different $Q^2 \rightarrow \infty$ limits. Fig. 5 contains the available data for the separated cross sections at $W > 2.5$ GeV. The biggest difference between the VR and RPR-2011 models is observed for the σ_{tr} and $\sigma_{\text{tr}'}$. The largest deviations between theory and data are found for the σ_{tr} and $\sigma_{\text{tr}'}$. The quantity and quality of the data, however, does not allow one to draw any definite conclusions.

From Figs. 4 and 5, one can easily see that in the VR model the anomalously large σ_u can be attributed to the R-P effects. An appealing feature of this approach is that $F_p(Q^2, s)$ can account for both the pion [3] and the kaon data at high energies and forward angles. It is worth mentioning that the RPR-2011 model does not adopt a proton EM transition form factor, i.e. $F_p^{\text{RPR}}(Q^2, s) = 1$. As a competing explanation for the observed trends in the Q^2 evolution of the data, a hard form factor is in-

troduced at the K and K^* EM vertices of the RPR-2011 model:

$$\Lambda_{\gamma KK}^{\text{RPR}} = \Lambda_{\gamma K^* K}^{\text{RPR}} = 1.3 \text{ GeV}. \quad (29)$$

For the K , this is a considerably larger cutoff energy than the measured value of Eq. (19) and considerably increases the longitudinal and transverse responses of the computed $p(\gamma^*, K^+)\Lambda$ cross sections. In a similar vein, the VGL model adopts [6]

$$\Lambda_{\gamma KK}^{\text{VGL}} = \Lambda_{\gamma K^* K}^{\text{VGL}} \approx 1.2 \text{ GeV}. \quad (30)$$

Guidal *et al.* argue that for the K this could be attributed to the fact that the pole in the kaon propagator $(t - m_K^2)^{-1}$ is

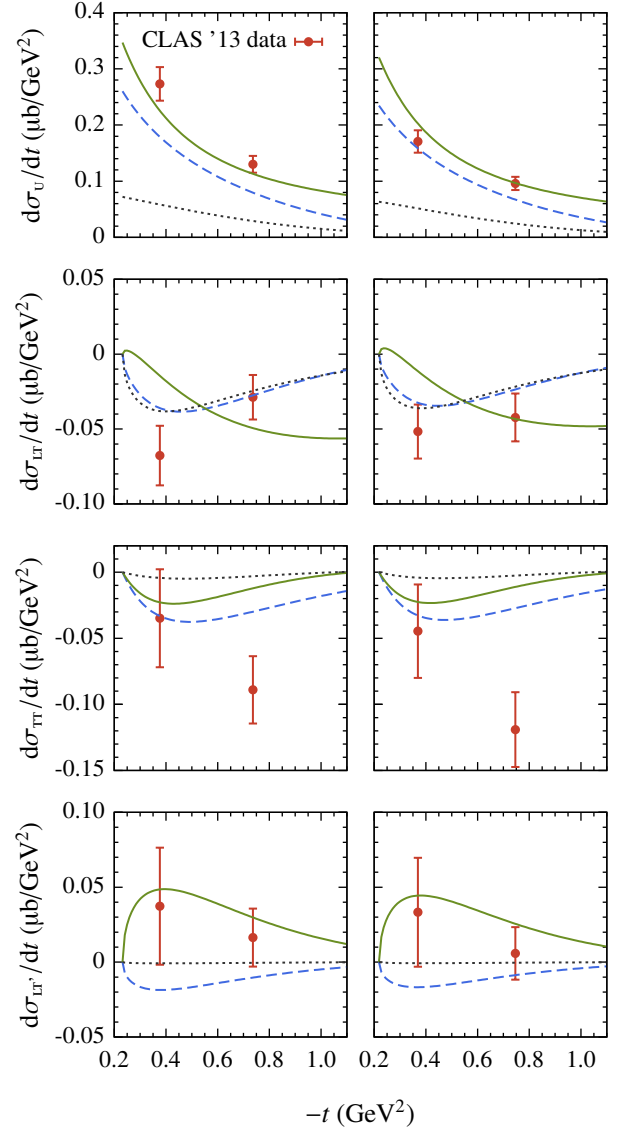


FIG. 5. (Color online) The $-t$ dependence of the $p(\gamma^*, K^+)\Lambda$ unseparated cross section $d\sigma_u/dt$ and the separated cross sections $d\sigma_{\text{tr}}/dt$, $d\sigma_{\text{tr}'}/dt$, and $d\sigma_{\text{tr}''}/dt$ at $E_e = 5.499$ GeV and $Q^2 = 1.80$ GeV² for $W = 2.525$ GeV (left) and $W = 2.575$ GeV (right). Curve notations of Fig. 4 are used. The data are from Ref. [21].

further from the physical region, compared to the pion case $(t - m_\pi^2)^{-1}$. Hence, the high $\Lambda_{\gamma KK}$ value would be representative for the whole kaon-Regge trajectory, rather than for the physical kaon.

Figures 6 and 7 show the VR and RPR-2011 predictions for the $p(\gamma^*, K^+)\Lambda$ L-T-separation experiment planned for the 12 GeV upgrade at JLab [8]. From both figures it is clear that the VR model predicts both substantially smaller longitudinal and larger transverse cross sections than the RPR-2011 model. For the σ_L this can be mainly attributed to the adopted values of $\Lambda_{\gamma KK}$ and to a smaller extent of $\Lambda_{\gamma K^*K}$. In particular at small $-t$, where t -channel K exchange is dominant, the magnitude of σ_L is very sensitive to the value of $\Lambda_{\gamma KK}$. On the

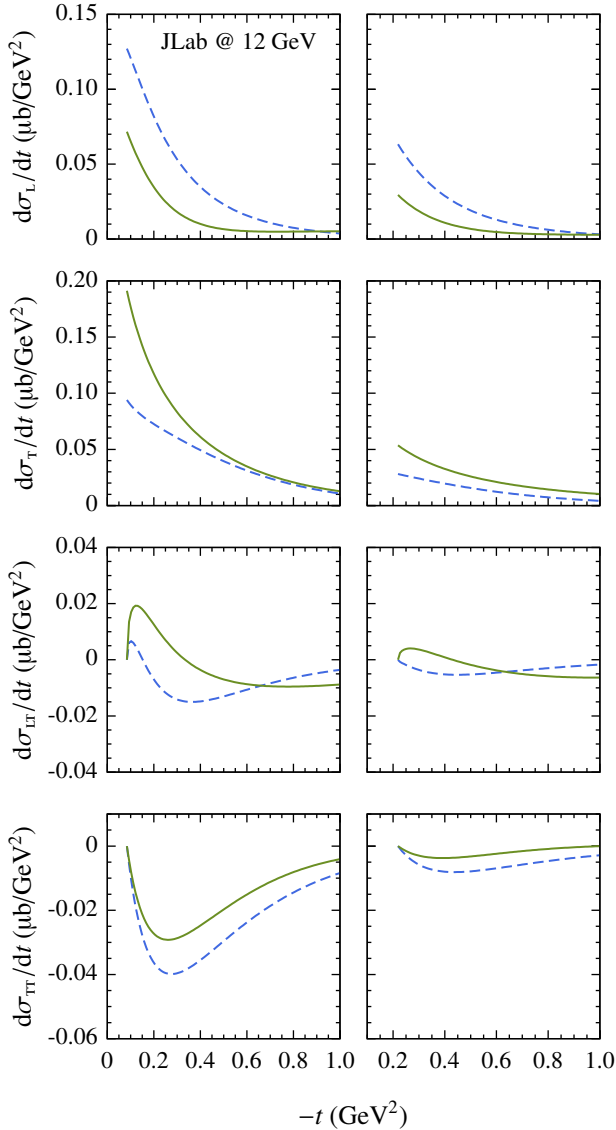


FIG. 6. (Color online) The $-t$ dependence of the separated $p(\gamma^*, K^+)\Lambda$ cross sections $d\sigma_L/dt$, $d\sigma_T/dt$, $d\sigma_{LT}/dt$, and $d\sigma_{TT}/dt$ at $W = 3.14$ GeV for $Q^2 = 1.25$ GeV^2 (left) and $Q^2 = 3.00$ GeV^2 (right). Curve notations of Fig. 4 are used. These are predictions for the planned $p(\gamma^*, K^+)\Lambda$ L-T-separation experiment [8].

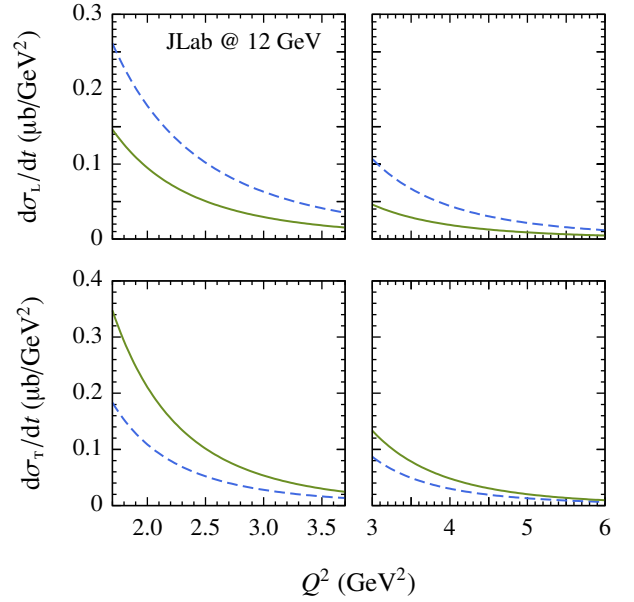


FIG. 7. (Color online) The Q^2 dependence of the separated $p(\gamma^*, K^+)\Lambda$ cross sections $d\sigma_L/dt$, $d\sigma_T/dt$, $d\sigma_{LT}/dt$, and $d\sigma_{TT}/dt$ at $t = t_{\min}$ for $x_B = 0.25$ (left) and $x_B = 0.40$ (right), with x_B being the Bjorken scaling variable. For the shown Q^2 ranges, one has $2.45 \text{ GeV} \lesssim W \lesssim 3.46 \text{ GeV}$ and $0.21 \text{ GeV}^2 \lesssim -t \lesssim 0.25 \text{ GeV}^2$ for $x_B = 0.25$, and $2.32 \text{ GeV} \lesssim W \lesssim 3.14 \text{ GeV}$ and $0.50 \text{ GeV}^2 \lesssim -t \lesssim 0.53 \text{ GeV}^2$ for $x_B = 0.40$. Curve notations of Fig. 4 are used. These are predictions for the planned $p(\gamma^*, K^+)\Lambda$ L-T-separation experiment of Ref. [8].

other hand, the larger transverse response in the VR model can be attributed to the R-P contributions in the gauge-fixing s channel. This is a key element of the VR framework and is not present in the RPR-2011 and the VGL model.

In π^+n electroproduction, hadronic models like the VGL model cannot account for the anomalously large σ_T above the resonance region [1]. A similar scenario is expected in high-energy $K^+\Lambda$ electroproduction. Indeed, when adopting the experimental value of Eq. (19) for $\Lambda_{\gamma KK}$, the VGL model, for example, significantly underpredicts the unseparated Cornell data shown in Fig. 4. Also the VR model without R-P effects substantially underpredicts these data (Figs. 4 and 5). Given that $\sigma_U = \sigma_T + \epsilon\sigma_L$ and that $\Lambda_{\gamma KK}$ predominantly influences σ_L at forward scattering, the much larger kaon cutoff energy required by the VGL model might actually be a compensation for an increased transverse response which remains unrevealed in σ_U . In this respect, the VR framework constitutes a promising approach as it inherently accounts for a larger σ_T and already successfully explains the separated structure functions, measured in high-energy pion electroproduction [3].

The JLab L-T-separation experiment for high-energy $K^+\Lambda$ electroproduction is expected to settle the magnitude of the σ_T response. In addition, the measurement of σ_L at small $-t$ will provide access to the value of $\Lambda_{\gamma KK}$ in off-shell circumstances. Another experiment is planned with the 12 GeV upgrade at JLab. The CLAS Collaboration intends to obtain the interference structure functions σ_{LT} , σ_{TT} , and $\sigma_{LT'}$ for Q^2 and

W values up to 12 GeV² and 3 GeV [27]. These data will also constitute an important test bed for the VR model as the proposed kinematics cover the trans-resonance region.

V. CONCLUSION AND OUTLOOK

Building on the VR model for charged-pion electroproduction, the VR model for the $p(\gamma^*, K^+)\Lambda$ reaction above the resonance region and forward angles ($-t < 1$ GeV²) was introduced. This model uses a three-trajectory Regge model for the photoproduction reaction as a starting base. The model features one pseudoscalar- and two vector-kaon Regge trajectories in the t channel. It provides an excellent description of the high-energy ($W > 2.6$ GeV), forward-angle ($\cos\theta_K^* > 0.35$) cross section and recoil polarization $p(\gamma, K^+)\Lambda$ data from the CLAS Collaboration. Turning to finite photon virtualities, a key feature of the VR model for $p(\gamma^*, K^+)\Lambda$ is to introduce a proton EM transition form factor, accounting for the contributions of resonances-partons connected to the highly off-shell proton in the gauge-fixing s -channel. The same proton transition form factor is assumed in both π^+n and $K^+\Lambda$ electroproduction. The magnitude of the antishrinkage effect in the s -channel is the sole parameter of the VR model and was optimized against the scarce $p(\gamma^*, K^+)\Lambda$ data. Remarkably, its optimized value coincides with the one obtained in pion electroproduction, for which far more data is available.

After introducing the R-P contributions, a good theory-experiment agreement is achieved for the 19 unseparated $p(\gamma^*, K^+)\Lambda$ cross-section data σ_U for $W > 2.5$ GeV and $-t \lesssim 1$ GeV². To date, only six data points are available for the interference structure functions. Due to limited statistics, the situation is rather inconclusive for those. An alternate explanation of the anomalous magnitude of the measured σ_U is that the kaon electromagnetic form factor in t -channel $p(\gamma^*, K^+)\Lambda$ is substantially harder than in elastic eK scattering.

Predictions are provided for the upcoming L-T-separation experiment at JLab. This experiment will provide the first data for the $p(\gamma^*, K^+)\Lambda$ longitudinal and transverse responses above the resonance region. It is expected that the forward-scattering σ_L data will map the kaon electromagnetic form factor in $K^+\Lambda$ electroproduction. The σ_T data, on the other hand, will reveal the importance of additional model features, like the role of resonance-parton effects. In high-energy pion electroproduction these provide a natural explanation for the observed magnitude of the transverse response. It is to be awaited whether or not this is the case in kaon electroproduction.

ACKNOWLEDGMENTS

This work is supported by the Research Council of Ghent University and the Flemish Research Foundation (FWO Vlaanderen). The authors would like to thank Daniel Carman and Viktor Mokeev for providing the recent $K^+\Lambda$ electroproduction data from the CLAS Collaboration and for useful

discussions.

Appendix: Observables

1. Photoproduction

The laboratory frame coordinate system is defined as

$$\mathbf{z} = \frac{\mathbf{q}}{|\mathbf{q}|}, \quad \mathbf{y} = \frac{\mathbf{q} \times \mathbf{k}'}{|\mathbf{q} \times \mathbf{k}'|}, \quad \mathbf{x} = \mathbf{y} \times \mathbf{z}, \quad (\text{A.1})$$

where \mathbf{q} and \mathbf{k}' are the three-momenta of the photon and outgoing kaon. The hadronic matrix elements $M_{\lambda_p, \lambda_\Lambda}^\lambda$ are defined as

$$M_{\lambda_p, \lambda_\Lambda}^\lambda = \epsilon_\mu^\lambda J_{\lambda_p, \lambda_\Lambda}^\mu, \quad (\text{A.2})$$

with $J_{\lambda_p, \lambda_\Lambda}^\mu$ being the transition current of the $p(\gamma^{(*)}, K^+)\Lambda$ reaction and ϵ_μ^λ the covariant polarization four-vector of the $\gamma^{(*)}$. For the observables covered in this work, it suffices to consider circularly polarized photons:

$$\epsilon_\mu^\pm = \frac{1}{\sqrt{2}}(0, \pm 1, i, 0). \quad (\text{A.3})$$

The unpolarized $p(\gamma, K^+)\Lambda$ differential cross section is calculated as

$$\frac{d\sigma}{d\Omega_K^*} = \frac{\alpha_e m_p m_\Lambda |\mathbf{k}'^*|}{16\pi W(s - m_p^2)} \sum_{\lambda, \lambda_p, \lambda_\Lambda} |M_{\lambda_p, \lambda_\Lambda}^\lambda|^2, \quad (\text{A.4})$$

where

$$|\mathbf{k}'^*| = \sqrt{\frac{(s + m_K^2 - m_\Lambda^2)^2}{4s} - m_K^2}, \quad (\text{A.5})$$

is the size of the three-momentum of the outgoing kaon in the center-of-mass frame. In terms of the hadronic matrix elements, the recoil polarization P reads

$$P = \frac{\sum_{\lambda, \lambda_p} (|M_{\lambda_p, \lambda_\Lambda=+y}^\lambda|^2 - |M_{\lambda_p, \lambda_\Lambda=-y}^\lambda|^2)}{\sum_{\lambda, \lambda_p, \lambda_\Lambda} |M_{\lambda_p, \lambda_\Lambda}^\lambda|^2}. \quad (\text{A.6})$$

2. Electroproduction

In electroproduction, the photon is virtual and a longitudinal polarization is allowed:

$$\epsilon_\mu^0 = \frac{1}{\sqrt{Q^2}}(\sqrt{v^2 + Q^2}, 0, 0, -v), \quad (\text{A.7})$$

with $v = E_e - E_{e'}$ being the energy difference between the initial and final electrons, e and e' . The unseparated differential cross section reads

$$\frac{d\sigma_U}{dt} = \frac{d\sigma_T}{dt} + \varepsilon \frac{d\sigma_L}{dt}, \quad (\text{A.8})$$

with ε given by

$$\varepsilon = \frac{4E_e E_{e'} - Q^2}{2(E_e^2 + E_{e'}^2) + Q^2}. \quad (\text{A.9})$$

The longitudinal and transverse structure functions are calculated as

$$\begin{aligned} \frac{d\sigma_L}{dt} &= 2\eta H_{0,0}, \\ \frac{d\sigma_T}{dt} &= \eta(H_{+,+} + H_{-,-}), \end{aligned} \quad (\text{A.10})$$

where

$$H_{\lambda,\lambda'} = \sum_{\lambda_p, \lambda_\Lambda} M_{\lambda_p, \lambda_\Lambda}^\lambda (M_{\lambda_p, \lambda_\Lambda}^{\lambda'})^*. \quad (\text{A.11})$$

The normalization factor η reads

$$\eta = \frac{\alpha_e m_p m_\Lambda}{4W(s - m_p^2)|\mathbf{q}^*|}, \quad (\text{A.12})$$

with

$$|\mathbf{q}^*| = \sqrt{\frac{(m_p^2 - s + Q^2)^2}{4s} + Q^2}, \quad (\text{A.13})$$

being the size of the photon's three-momentum in the center-of-mass frame. The interference structure functions for the longitudinal and transverse components of the virtual photon polarization can be expressed as

$$\begin{aligned} \frac{d\sigma_{LT}}{dt} &= -\eta(H_{+,0} + H_{0,+} - H_{0,-} - H_{-,0}), \\ \frac{d\sigma_{TT}}{dt} &= -\eta(H_{+,-} + H_{-,+}), \\ \frac{d\sigma_{LT'}}{dt} &= -\eta(H_{+,0} - H_{0,+} + H_{0,-} - H_{-,0}). \end{aligned} \quad (\text{A.14})$$

Finally, the transformation from dt to $d\Omega_K^*$ can be accomplished by employing the relation

$$\frac{d\Omega_K^*}{dt} = \frac{\pi}{|\mathbf{q}^*||\mathbf{k}^*|}. \quad (\text{A.15})$$

Note that, strictly speaking, the differential “ dt ” in Eqs. (A.8), (A.10), (A.14) and (A.15) should read “ $-dt$ ”. It is a conventional, however, to write “ dt ” in the expressions for the differential cross sections.

-
- [1] H. P. Blok *et al.*, *Phys. Rev. C* **78**, 045202 (2008).
 - [2] M. M. Kaskulov and U. Mosel, *Phys. Rev. C* **81**, 045202 (2010).
 - [3] T. Vranckx and J. Ryckebusch, *Phys. Rev. C* **89**, 025203 (2014).
 - [4] M. Guidal, J. M. Laget, and M. Vanderhaeghen, *Nucl. Phys. A* **627**, 645 (1997).
 - [5] M. Vanderhaeghen, M. Guidal, and J. M. Laget, *Phys. Rev. C* **57**, 1454 (1998).
 - [6] M. Guidal, J. M. Laget, and M. Vanderhaeghen, *Phys. Rev. C* **61**, 025204 (2000).
 - [7] M. Guidal, J. M. Laget, and M. Vanderhaeghen, *Phys. Rev. C* **68**, 058201 (2003).
 - [8] T. Horn *et al.*, *JLab PAC* **34**, PR12-09-011 (2009).
 - [9] T. Corthals, J. Ryckebusch, and T. Van Cauteren, *Phys. Rev. C* **73**, 045207 (2006).
 - [10] T. Corthals, T. Van Cauteren, P. Van Craeyveld, J. Ryckebusch, and D. G. Ireland, *Phys. Lett. B* **656**, 186 (2007).
 - [11] L. De Cruz, T. Vranckx, P. Vancraeyveld, and J. Ryckebusch, *Phys. Rev. Lett.* **108**, 182002 (2012).
 - [12] L. De Cruz, J. Ryckebusch, T. Vranckx, and P. Vancraeyveld, *Phys. Rev. C* **86**, 015212 (2012).
 - [13] J. Beringer *et al.* [Particle Data Group Collaboration], *Phys. Rev. D* **86**, 010001 (2012).
 - [14] T. Corthals, D. G. Ireland, T. Van Cauteren, and J. Ryckebusch, *Phys. Rev. C* **75**, 045204 (2007).
 - [15] P. Vancraeyveld, *Ph. D. thesis*, Ghent University (2011).
 - [16] M. E. McCracken *et al.* [CLAS Collaboration], *Phys. Rev. C* **81**, 025201 (2010).
 - [17] S. A. Ivashyn and A. Y. Korchin, *Eur. Phys. J. C* **49**, 697 (2007).
 - [18] C. J. Bebek *et al.*, *Phys. Rev. Lett.* **32**, 21 (1974).
 - [19] C. J. Bebek, C. N. Brown, P. Bucksbaum, M. Herzlinger, S. D. Holmes, C. A. Lichtenstein, F. M. Pipkin, S. W. Raither, and L. K. Sisterson, *Phys. Rev. D* **15**, 594 (1977).
 - [20] C. J. Bebek, A. Browman, C. N. Brown, K. M. Hanson, R. V. Kline, D. Larson, F. M. Pipkin, S. W. Raither, A. Silberman, and L. K. Sisterson, *Phys. Rev. D* **15**, 3082 (1977).
 - [21] D. S. Carman *et al.* [CLAS Collaboration], *Phys. Rev. C* **87**, 025204 (2013).
 - [22] R. M. Moring *et al.* [E93018 Collaboration], *Phys. Rev. C* **67**, 055205 (2003).
 - [23] P. Ambrozewicz *et al.* [CLAS Collaboration], *Phys. Rev. C* **75**, 045203 (2007).
 - [24] R. Nasseripour *et al.* [CLAS Collaboration], *Phys. Rev. C* **77**, 065208 (2008).
 - [25] D. S. Carman *et al.* [CLAS Collaboration], *Phys. Rev. C* **79**, 065205 (2009).
 - [26] M. Coman *et al.* [Jefferson Lab Hall A Collaboration], *Phys. Rev. C* **81**, 052201 (2010).
 - [27] D. S. Carman, R. Gothe, and V. Mokeev [CLAS Collaboration], Private communication.